Research Article Vol. 6, No. 9 / September 2019 / Optica 1117

Resonantly enhanced nonreciprocal silicon Brillouin amplifier

Nils T. Otterstrom,[1,4] Eric A. Kittlaus,[1] Shai Gertler,[1] Ryan O. Behunin,[2] Anthony L. Lentine,[3] and Peter T. Rakich[1,5]

[1]Department of Applied Physics, Yale University, New Haven, Connecticut 06520, USA
[2]Department of Physics and Astronomy, Northern Arizona University, Flagstaff, Arizona 86001, USA
[3]Applied Photonic Microsystems, Sandia National Laboratories, Albuquerque, New Mexico 87185, USA
[4]e-mail: nils.otterstrom@yale.edu
[5]e-mail: peter.rakich@yale.edu

Received 11 March 2019; revised 17 June 2019; accepted 15 July 2019 (Doc. ID 362022); published 27 August 2019

The ability to amplify light within silicon waveguides is central to the development of high-performance silicon photonic device technologies. To this end, the large optical nonlinearities made possible through stimulated Brillouin scattering offer a promising avenue for power-efficient all-silicon amplifiers, with recent demonstrations producing several dB of net amplification. However, scaling the degree of amplification to technologically compelling levels (>10 dB), necessary for everything from filtering to small signal detection, remains an important goal. Here, we significantly enhance the Brillouin amplification process by harnessing an intermodal Brillouin interaction within a multi-spatial-mode silicon racetrack resonator. Using this approach, we demonstrate more than 20 dB of net Brillouin amplification in silicon, advancing state-of-the-art performance in silicon waveguides by a factor of 30. This level of amplification is achieved with modest (~15 mW) continuous-wave pump powers and produces low out-of-band noise. Moreover, we show that this same system behaves as a unidirectional amplifier, providing more than 28 dB of optical nonreciprocity without insertion loss in an all-silicon platform. Building on these results, this device concept opens the door to new types of all-silicon injection-locked Brillouin lasers, high-performance photonic filters, and waveguide-compatible distributed optomechanical phenomena.

https://doi.org/10.1364/OPTICA.6.001117

1. INTRODUCTION

High-performance optical amplification is an essential functionality in integrated photonic circuits. Within the context of silicon photonics, however, strategies for robust integrated amplifiers have faced significant challenges that stem from silicon's indirect bandgap and high levels of nonlinear loss [1,2]. To date, silicon amplifier technologies have relied on either hybrid integration strategies [3–6] or nonlinear optical interactions [1] such as Raman [7–10] or Kerr effects [11–13]. While Raman and Kerr interactions have been used to produce net amplification using pulsed optical pumping [7–11], active electrical removal of free carriers [14], or large mid-IR pump powers [12,13], it remains nontrivial to achieve large degrees of power-efficient optical amplification due to the competition between gain and nonlinear absorption in silicon.

Recently, the nonlinear light–sound coupling known as stimulated Brillouin scattering has emerged as a promising mechanism for optical amplification in silicon, with dynamics and performance that can be customized through structural control [15,16]. Once entirely absent from silicon photonics, these Brillouin interactions have emerged as one of the strongest and most tailorable nonlinearities in silicon [16,17], permitting net optical amplification [18–20] and Brillouin lasing in silicon photonic circuits [21]. While recent demonstrations have achieved 2–5 dB of amplification [19,20], scaling the amplification to levels necessary for high-fidelity filtering [22–25] and small-signal detection schemes [26] remains a nontrivial challenge [27].

In this paper, we demonstrate record-high Brillouin gain and amplification in silicon through a resonantly enhanced Brillouin interaction. This all-silicon amplifier system is based on a stimulated intermodal Brillouin scattering process, in which a traveling elastic wave mediates nonlinear energy transfer between light waves propagating in distinct optical spatial modes [20]. Building on existing device concepts for silicon Brillouin lasers [21], we harness and dramatically enhance this stimulated Brillouin process using a multi-spatial-mode racetrack resonator system that is interfaced with mode-specific couplers to allow signal light to be amplified as it is transmitted through the system. We use this device to realize 30 dB of Brillouin gain, corresponding to over 20 dB of net Brillouin amplification. This resonantly enhanced amplifier advances state-of-the-art net amplification in silicon waveguides by 15 dB, representing a 30-fold improvement [19], and offers complimentary capabilities to hybrid chalcogenide–silicon systems [28] for high-performance Brillouin-photonic technologies. Leveraging the unidirectional amplification produced by this phase-matched

process, we also use this system to demonstrate more than 28 dB of nonreciprocal contrast between forward- and backward-propagating waves. This scheme provides robust optical nonreciprocity without insertion loss. Beyond the results presented here, this device concept is a stepping stone toward chip-integrated injection-locked Brillouin lasers, microwave photonic filtering techniques, and distributed optomechanical phenomena.

2. RESULTS

We use a resonant optical configuration to produce greatly enhanced intermodal Brillouin amplification and optical nonreciprocity in an all-silicon structure. This strategy allows us to transform the otherwise modest amplification (~2 dB) possible in a linear geometry (using a waveguide of the same design; see Ref. [20]), into more than 20 dB of net amplification. We achieve this significant enhancement in performance by leveraging the resonator geometry diagrammed in Fig. 1(a) that builds upon the laser structure described in Ref. [21]. In this type of configuration, resonant transmission through the system becomes lossless (i.e., approaches unity) if the internal gain produced by stimulated intermodal Brillouin scattering balances the internal losses of the resonator. In the case when the gain exceeds the internal losses of the resonator, but does not exceed the total loss (i.e., internal + external), the system can yield greater-than-unity transmission without producing self-oscillation (i.e., below the laser threshold). In the limit when the gain approaches the total loss of the system, the resonantly enhanced amplification can become arbitrarily large—in principle, limited only by gain depletion. Furthermore, we show that due to the phase-matching requirements of the stimulated intermodal Brillouin process, this resonantly enhanced amplification is unidirectional, yielding significant optical nonreciprocity.

The resonantly enhanced Brillouin amplifier consists of a 15-mm-long racetrack cavity that possesses two Brillouin-active regions [Fig. 1(a)]. The device is fabricated from a single-crystal SOI wafer using a hybrid CMOS-MEMS process (see Supplement 1, Section 3.C). The racetrack cavity is formed from a multimode silicon ridge waveguide that supports low-loss guidance of transverse electric (TE)-like symmetric and antisymmetric optical spatial modes. In the Brillouin-active regions, this multimode optical waveguide is suspended to provide acoustic guidance for the 6 GHz traveling elastic wave that mediates strong intermodal Brillouin coupling [see Fig. 1(b); for waveguide dimensions, see Supplement 1, Section 3.C]. Within the resonator, the symmetric and antisymmetric optical spatial modes form two distinct sets of resonances. The symmetric spatial mode produces a set of high-Q factor ($Q_1 = 10^6$) cavity modes centered at frequencies $\{\omega_1^n\}$ while the antisymmetric spatial mode produces

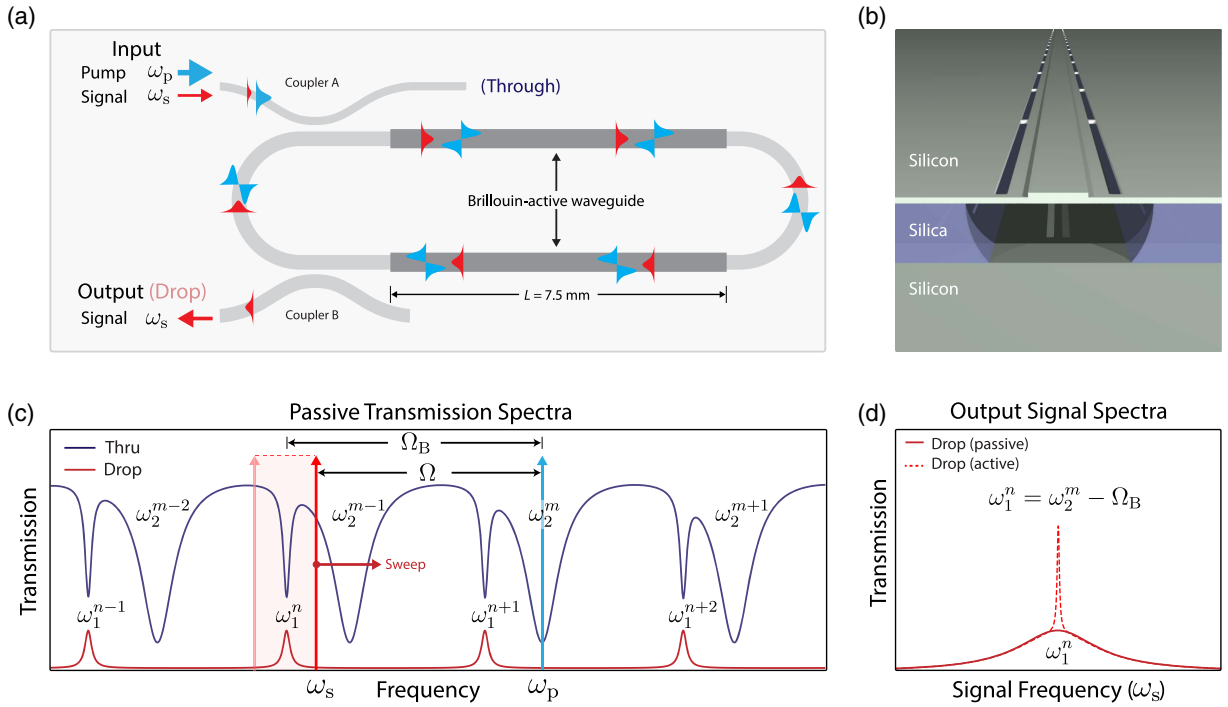

Fig. 1. (a) Resonantly enhanced Brillouin amplifier device concept and operation scheme. The amplifier is composed of a multi-spatial-mode racetrack resonator with two Brillouin-active regions. Using the frequency selectivity of the cavity, pump (ω_p) and signal waves (ω_s) are coupled into the antisymmetric and symmetric cavity modes, respectively, via a multimode coupler. As the pump and signal waves traverse the Brillouin-active segments, the pump wave resonantly amplifies the signal wave through stimulated intermodal Brillouin scattering. The signal wave exits the system through a mode-selective coupler (drop port), which is designed to couple strongly to the symmetric mode and weakly to the antisymmetric mode. (b) Schematic illustrating the cross-sectional geometry of the Brillouin-active regions. This suspended multimode silicon waveguide supports two transverse electric (TE)-like optical spatial modes and a 6 GHz antisymmetric Lamb-like elastic wave, which mediates intermodal Brillouin amplification. (c) Idealized optical transmission spectra at the through and drop ports. Coupling into the racetrack resonator via a multimode coupler yields a characteristic multimode transmission spectrum at the through port, with broad (centered at ω_2^m) and narrow (centered at ω_1^n) resonances corresponding to the antisymmetric and symmetric optical spatial modes, respectively. The mode-selective drop port is designed to couple out only the symmetric cavity modes. Resonantly enhanced Brillouin amplification measurements are performed by coupling the pump wave (ω_p) to an antisymmetric cavity mode (ω_2^m) and sweeping the signal wave (ω_s) through a symmetric cavity mode (ω_1^n) that is redshifted from by the Brillouin frequency (Ω_B). (d) Zoomed-in transmission spectrum for the signal wave exiting the drop port when $\omega_s \approx \omega_1^n$ with (active) and without (passive) the Brillouin gain supplied by the pump wave.

a set of cavity modes having lower Q factors ($Q_2 = 2 \times 10^5$) at frequencies $\{\omega_2^m\}$.

To access these cavity modes, the resonator is interfaced with two different directional couplers that permit efficient, mode-specific coupling into and out of the resonator. The input coupler (coupler A) is designed to couple appreciably to both optical spatial modes, producing a characteristic cavity transmission (through) spectrum with two distinct sets of resonant features [see in Fig. 1(c)]. The broad (narrow) resonances correspond to the cavity modes produced by the antisymmetric (symmetric) optical spatial mode. Using the frequency selectivity of the resonator, the pump light (ω_p) is resonantly coupled into an antisymmetric cavity mode while the signal light (ω_s) is coupled into a symmetric cavity mode; to do this, we tune the pump and signal frequencies such that they satisfy the distinct cavity resonance conditions for a pair of antisymmetric and symmetric cavity modes, respectively. Signal light circulating in the symmetric cavity mode exits the resonator through a mode-selective coupler (coupler B), which preferentially couples to the symmetric spatial mode (see Supplement 1, Section 2 for details).

When the pump wave is resonant with an antisymmetric cavity mode ($\omega_p = \omega_2^m$) and a symmetric cavity mode satisfies the Brillouin condition ($\omega_1^n = \omega_2^m - \Omega_B$), signal light injected into the symmetric cavity mode (ω_1^n) can experience resonantly enhanced Brillouin amplification. Through experiments, we couple the pump and signal waves into the antisymmetric and symmetric cavity modes of the racetrack resonator via coupler A. Within the resonator, the copropagating pump and signal waves nonlinearly couple as they traverse the Brillouin-active regions of the racetrack, producing Brillouin energy transfer and single-sideband gain through stimulated intermodal Brillouin scattering [20]. As the pump power approaches the threshold for lasing, the amplification is significantly enhanced [see Fig. 1(d)].

A. Experimental Results

We characterize the resonantly enhanced Brillouin amplifier through nonlinear laser spectroscopy measurements using the setup diagrammed in Fig. 2(a). All measurements are performed at room temperature and atmospheric pressure using 1.54 μm optical wavelengths. In this experimental scheme, light from a tunable laser is split along two paths; the upper path is used to synthesize the pump and signal waves, while the lower arm is used to create an optical local oscillator (LO) for heterodyne analysis of the emitted signal wave. The optical LO (lower arm) is generated by an acousto-optic modulator, which blueshifts the light by $\Delta = 2\pi \times 44$ MHz. The upper path uses an intensity modulator (IM), erbium-doped fiber amplifier (EDFA), and variable optical attenuator (VOA) to synthesize pump and signal waves of a desired power and variable frequency detuning. Pump and signal waves are then coupled on-chip through a grating coupler; the light is subsequently routed to the racetrack

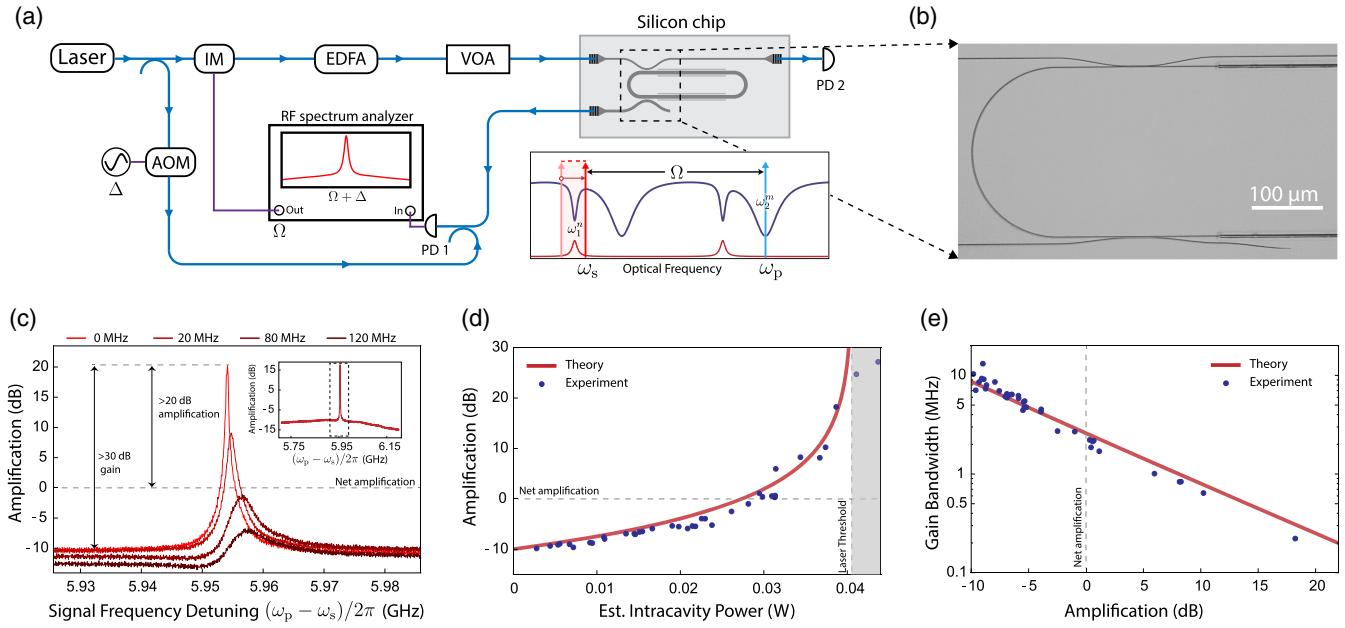

Fig. 2. (a) Diagram of the experimental apparatus used to characterize the resonantly enhanced Brillouin amplifier. Laser light is split along two paths. One path is used to synthesize an optical local oscillator (LO) using an acousto-optic modulator (AOM), which blueshifts the light by $\Delta = 2\pi \times 44$ MHz. The other arm synthesizes pump and signal waves with the desired frequency detuning ($\Omega = \omega_p - \omega_s$) and powers using an intensity modulator (IM), erbium-doped-fiber amplifier (EDFA), and variable optical attenuator (VOA); the light is subsequently coupled on-chip for nonlinear amplification measurements. After passing through the device, the signal wave is coupled through the drop port and off-chip, where it is combined with the blueshifted LO and measured on a high-speed photodetector (PD 1). The RF spectrum analyzer sweeps the detuning (Ω) and measures the microwave power at ($\Omega + \Delta$), permitting single-sideband measurements of $\omega_s = \omega_p - \Omega$ (without cross talk from light at $\omega_p + \Omega$). (b) Optical micrograph (in gray scale) showing a top-down view of part of the device. (c) Gain spectra as a function of signal wave detuning around the Brillouin resonance, showing more than 30 dB of gain and 20 dB of net amplification. Each trace represents a different estimated detuning of the optical cavity mode relative to the Brillouin frequency (see zoomed-out inset). Large optical cavity detunings relative to the Brillouin resonance result in lower amplification and characteristic asymmetric line shapes. (d) Measured and theoretical signal wave amplification produced over a range of intracavity powers. As the pump power approaches the laser threshold power, the resonantly enhanced Brillouin amplification increases dramatically. Data are compiled from a series of power, microwave frequency detuning, and wavelength sweeps (for more details see Supplement 1, Section 3.B). (e) Linewidth narrowing of the gain bandwidth as a function of signal wave amplification.

resonator through a single-mode waveguide. Signal light exiting the device is combined with the optical LO and measured using a high-speed photo-receiver for heterodyne spectral analysis. We sweep a microwave oscillator at Ω to synthesize the signal wave at $\omega_s = \omega_p - \Omega$, and synchronously detect at $\Omega + \Delta$ using a spectrum analyzer. By tracking at this offset frequency (Δ), we are able to selectively detect the redshifted signal wave ($\omega_p - \Omega$) without crosstalk from the blueshifted tone ($\omega_p + \Omega$).

Using this experimental configuration, we sweep the laser wavelength, pump power, and signal wave detuning to characterize the amplifier system. In the limit of low pump power, no Brillouin gain is produced, and we recover the linear resonant response produced by the symmetric mode of the racetrack cavity. When the pump power is increased, we observe a narrow gain peak at the Brillouin frequency atop the linear resonator response [see Fig. 1(d)]. As the pump power approaches the laser threshold power, we observe a dramatic increase in the level of resonantly enhanced amplification, consistent with our theoretical predictions [see Figs. 2(c)–2(d)]. Just below threshold, this resonantly enhanced interaction is sufficient to yield in excess of 30 dB of gain, representing more than 20 dB of net amplification after accounting for losses produced by linear transmission through the resonator [see Fig. 2(c)]. The degree of amplification depends strongly on the mode-pair detuning (i.e., the frequency separation $\omega_2^m - \omega_1^n$) relative to the Brillouin frequency, as shown in Fig. 2(c). In addition, we observe that the gain bandwidth scales inversely with the amplification as a result of gain narrowing, in agreement with theory [see Fig. 2(e)].

Owing to the phase-matching characteristics of this interband Brillouin process, we show that this system yields unidirectional gain that results in a highly nonreciprocal response. This is because the phonon required for the resonantly enhanced Brillouin process mediates gain between the copropagating pump and signal waves, but does not produce Brillouin coupling between counterpropagating waves [29,30]. We demonstrate these dynamics by coupling the pump wave into the antisymmetric resonator mode with a counterclockwise orientation; we then examine the reciprocity of the system by injecting the signal wave in the forward [Fig. 3(a)] and backward [Fig. 3(b)] directions such that the signal wave copropagates and counterpropagates with the pump wave within the resonator, respectively. When energy conservation is satisfied ($\omega_p = \omega_s + \Omega_B$), the forward configuration yields net amplification (red) of the signal wave, while the backward configuration yields net loss (gray) as a result of linear transmission through the cavity in the absence of gain. Using a fiber-coupled switch, we alternate between the forward and backward configurations while measuring the transmission as a function of signal wave detuning. As shown in Fig. 3(c), these measurements reveal a peak optical nonreciprocity of 28 dB and a bandwidth of 2.5 MHz over which the system provides >10 dB of optical isolation with no insertion loss (see Supplement 1, Section 3.A for more details).

B. Theory

To understand our observations, we develop a mean-field analytical model that captures the salient amplification and noise dynamics of this resonantly enhanced amplification process (for detailed derivation, see Supplement 1, Section 1). This model treats the pump, signal, and phonon fields as distinct modes that are nonlinearly coupled through stimulated intermodal Brillouin scattering. Taking a Fourier transform in time allows us to solve for the output signal spectrum $|S^{out}[\omega_s]|^2$ relative to the input signal spectrum $|S^{in}[\omega_s]|^2$, yielding

$$\frac{|S^{out}[\omega_s]|^2}{|S^{in}[\omega_s]|^2} = \left| \frac{\sqrt{\gamma_{A,1}}\sqrt{\gamma_{B,1}}}{-i(\omega_s - \omega_1^n) + \frac{\gamma_{tot,1}}{2} - \frac{G_B P v_{g,1} \Gamma/4}{i(\omega_p - \omega_s - \Omega_B) + \Gamma/2}} \right|^2, \quad (1)$$

where $\gamma_{tot,1}$ is the total loss rate for the symmetric spatial mode (defined by $\gamma_{tot,1} \equiv \gamma_{A,1} + \gamma_{B,1} + \alpha_1 v_{g,1}$), $\gamma_{(A,B),1}$ are the dissipation rates for the symmetric spatial mode due to couplers A and B

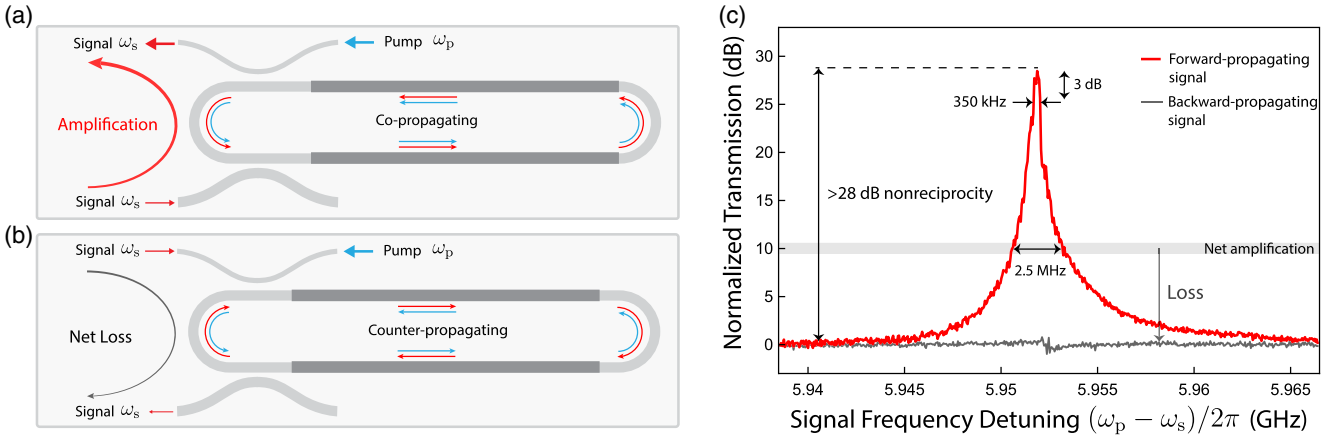

Fig. 3. Demonstration of unidirectional optical amplification and nonreciprocity (for experimental apparatus, see Supplement 1, Section 3.A) (a) Experimental arrangement for directional amplification. Pump and signal waves are injected through respective multimode (top) and mode-specific (bottom) couplers such that they copropagate (forward direction) within the resonator. This configuration allows pump and signal waves to nonlinearly couple through a stimulated forward intermodal Brillouin process, yielding net amplification of the signal wave. (b) By contrast, a signal wave propagating in the opposite (backward) direction does not experience Brillouin gain as a result of phase matching; the elastic wave that mediates forward intermodal scattering is not phase-matched to the backward-scattering process. Thus, in this backward configuration, the signal wave experiences net loss resulting from linear transmission through the resonator. (c) Experimental demonstration of unidirectional amplification. Signal transmission through the system in the forward (red, copropagating with the pump) and backward (gray; counterpropagating with the pump) directions as a function of signal frequency detuning $\Omega/2\pi$. This system yields a maximum 28 dB of nonreciprocity (with a FWHM of 350 kHz) and provides >10 dB of isolation over a 2.5 MHz bandwidth.

$(\gamma_{(A,B),1} \equiv -(2v_{g,1}/L)\ln(1-\mu^2_{(A,B),1})^{1/2})$, $v_{g,1}$ is the group velocity of the symmetric optical spatial mode, $\mu^2_{(A,B),1}$ is the coupling constant of couplers A or B for the symmetric spatial mode, L is the length of the racetrack resonator, P is the intracavity pump power, α_1 is the linear propagation loss of the symmetric spatial mode, G_B is the Brillouin gain coefficient, and Γ is the dissipation rate for the acoustic field.

Equation (1) can be used to self-consistently predict the amplification and gain bandwidth of the system and is the basis for the theoretical trends plotted in Figs. 2(d)–2(e). Using this framework, we also analyze the noise dynamics and gain depletion produced in this Brillouin amplifier (for detailed analysis of the noise figure and gain depletion, see Supplement 1 Sections 1.B–1.C). We note that Eq. (1) diverges at the laser threshold condition, which is an artifact of the stiff pump approximation in this analysis. While the equations are consistent with those describing parametric amplification in cavity-optomechanical systems [31], we note that this analysis requires a mean-field treatment of a distributed, heavily spatially damped phonon field, which is valid only in the presence of the pump and Stokes field (for further discussion, see Ref. [21]).

3. DISCUSSION

In this paper, we have demonstrated that a resonant optical configuration can be used to dramatically enhance the stimulated intermodal Brillouin scattering process, yielding record-high Brillouin gain and net amplification in an all-silicon chip-integrated system. These results represent a 500-fold improvement in gain and more than an 60× enhancement in net amplification relative to linear (nonresonant) devices of the same design [20]. Thanks to the highly efficient nature of the resonantly enhanced amplification process, this level of performance is achieved with minimal pump powers (∼15 mW incident and ∼40 mW intracavity), greatly reducing two-photon absorption (TPA) and TPA-induced free-carrier absorption (FCA) (estimated signal loss due to nonlinear effects is 0.1 dB) that otherwise inhibit large Brillouin amplification in linear silicon waveguides [20,27]. Moreover, the highly efficient operation of this device benefits from the unique phase-matching dynamics of intermodal Brillouin scattering, which intrinsically prohibit unwanted anti-Stokes [20,21] and four-wave mixing processes [32]. Building on this work, even greater optical amplification may be realized by increasing the passive signal transmission while maintaining a low laser threshold; this may be accomplished through further optimization of the mode-specific coupler design or multimode optomechanical waveguide. Further improvements may also include the use of integrated heaters—a standard capability in silicon photonic systems [33]—to allow flexible and reconfigurable tuning of the Brillouin gain, permitting tunable operation over the entire C band.

As a byproduct of this resonantly enhanced interaction, we also show that this process yields characteristic narrowing of the gain bandwidth (from 10 MHz to sub-MHz) as the pump power approaches the laser threshold power. While broadband amplification is desirable for many applications, the narrowband amplification produced through this resonantly enhanced system presents its own set of intriguing opportunities. In contrast to broadband amplification, in which spontaneous emission or scattering can produce substantial noise over an equally large bandwidth, the narrowband nature of the interaction yields low out-of-band noise (for details, see Supplement 1, Section 1.B). In addition, the narrow, tailorable nature of the gain bandwidth could prove advantageous for many on-chip functionalities, including narrowband optical and microwave photonic filters [22,23], carrier recovery for microwave photonic signal processing [34], and tunable time delay [31,35–37].

In addition, the unidirectional nature of this Brillouin amplifier could enable new types of all-silicon, chip-integrated nonreciprocal technologies. These nonreciprocal dynamics are closely related to those recently demonstrated in cavity-optomechanical and nonlinear optical systems, where time modulation produced through a parametric coupling can produce directional absorption or amplification [38,39]. While similar behaviors have been demonstrated in glass microresonators [40–44], photonic crystal fibers [29], and in silicon optomechanical crystals at cryogenic temperatures [45], this form of nonreciprocity has not previously been demonstrated in a silicon system at room temperature. Moreover, though narrowband in comparison, the level of nonreciprocity demonstrated here (∼30 dB) is competitive with that achievable using integrated magneto-optic [46–49] or acousto-optic strategies [50,51]. While magneto-optic-based silicon-photonic isolator and circulator technologies are advancing steadily, they require complex fabrication techniques [46–49]. Acousto-optic strategies are also very promising; however, they have yet to achieve efficiencies necessary to produce optical isolation with low insertion losses [50,51]. As such, the optical nonreciprocity we demonstrate here—in an all-silicon device with no insertion loss—represents an important step towards practical isolator and circulator technologies in silicon photonics.

In summary, we have demonstrated record-high Brillouin gain and amplification in an integrated silicon photonic circuit. This device is capable of delivering more than 30 dB of gain and 20 dB of net amplification, representing a 30-fold improvement over state-of-the-art performance [19]. Moreover, we show that this phase-matched stimulated Brillouin process is intrinsically unidirectional, yielding more than 28 dB of nonreciprocal contrast between forward- and backward-propagating waves. These results represent an important milestone for Brillouin-based amplifier and isolator technologies in silicon photonics and enable new schemes for high-performance microwave photonic filtering, tunable time delay, and injection-locked Brillouin lasers.

Funding. National Science Foundation (NSF) (DGE1122492, Graduate Research Fellowship); David and Lucile Packard Foundation; Sandia National Laboratories (DE-NA-0003525).

Acknowledgment. We thank Prashanta Kharel for valuable discussions and for assistance in developing the experimental apparatus. This material is based upon work supported by the Packard Fellowship for Science and Engineering, the National Science Foundation Graduate Research Fellowship under Grant No. DGE1122492 (N.T.O.), and the Laboratory Directed Research and Development program at Sandia National Laboratories. Sandia National Laboratories is a multi-program laboratory managed and operated by National Technology and Engineering Solutions of Sandia, LLC., a wholly owned subsidiary of Honeywell International, Inc., for the U.S. Department of Energy's National Nuclear Security Administration under contract DE-NA-0003525. This paper describes objective technical results and analysis. Any subjective views or opinions that might

be expressed in the paper do not necessarily represent the views of the U.S. Department of Energy, the National Science Foundation, or the United States Government.

See Supplement 1 for supporting content.

REFERENCES

1. J. Leuthold, C. Koos, and W. Freude, "Nonlinear silicon photonics," Nat. Photonics **4**, 535–544 (2010).
2. D. Liang and J. E. Bowers, "Recent progress in lasers on silicon," Nat. Photonics **4**, 511–517 (2010).
3. H. Park, A. W. Fang, O. Cohen, R. Jones, M. J. Paniccia, and J. E. Bowers, "A hybrid AlGaInAs–silicon evanescent amplifier," IEEE Photon. Technol. Lett. **19**, 230–232 (2007).
4. M. J. Heck, H.-W. Chen, A. W. Fang, B. R. Koch, D. Liang, H. Park, M. N. Sysak, and J. E. Bowers, "Hybrid silicon photonics for optical interconnects," IEEE J. Sel. Top. Quantum Electron. **17**, 333–346 (2011).
5. S. Keyvaninia, G. Roelkens, D. Van Thourhout, M. Lamponi, F. Lelarge, J.-M. Fedeli, S. Messaoudene, E. Geluk, and B. Smalbrugge, "A highly efficient electrically pumped optical amplifier integrated on a SOI waveguide circuit," in *IEEE 9th International Conference on Group IV Photonics (GFP)* (IEEE, 2012), pp. 222–224.
6. L. Agazzi, J. D. Bradley, M. Dijkstra, F. Ay, G. Roelkens, R. Baets, K. Wörhoff, and M. Pollnau, "Monolithic integration of erbium-doped amplifiers with silicon-on-insulator waveguides," Opt. Express **18**, 27703–27711 (2010).
7. R. Claps, D. Dimitropoulos, V. Raghunathan, Y. Han, and B. Jalali, "Observation of stimulated Raman amplification in silicon waveguides," Opt. Express **11**, 1731–1739 (2003).
8. O. Boyraz and B. Jalali, "Demonstration of 11 dB fiber-to-fiber gain in a silicon Raman amplifier," IEICE Electron. Express **1**, 429–434 (2004).
9. T. Liang and H. Tsang, "Efficient Raman amplification in silicon-on-insulator waveguides," Appl. Phys. Lett. **85**, 3343–3345 (2004).
10. A. Liu, H. Rong, M. Paniccia, O. Cohen, and D. Hak, "Net optical gain in a low loss silicon-on-insulator waveguide by stimulated Raman scattering," Opt. Express **12**, 4261–4268 (2004).
11. M. A. Foster, A. C. Turner, J. E. Sharping, B. S. Schmidt, M. Lipson, and A. L. Gaeta, "Broad-band optical parametric gain on a silicon photonic chip," Nature **441**, 960–963 (2006).
12. X. Liu, R. M. Osgood, Jr., Y. A. Vlasov, and W. M. Green, "Mid-infrared optical parametric amplifier using silicon nanophotonic waveguides," Nat. Photonics **4**, 557–560 (2010).
13. B. Kuyken, X. Liu, G. Roelkens, R. Baets, R. M. Osgood, Jr., and W. M. Green, "50 dB parametric on-chip gain in silicon photonic wires," Opt. Lett. **36**, 4401–4403 (2011).
14. H. Rong, R. Jones, A. Liu, O. Cohen, D. Hak, A. Fang, and M. Paniccia, "A continuous-wave Raman silicon laser," Nature **433**, 725–728 (2005).
15. P. T. Rakich, C. Reinke, R. Camacho, P. Davids, and Z. Wang, "Giant enhancement of stimulated Brillouin scattering in the subwavelength limit," Phys. Rev. X **2**, 011008 (2012).
16. H. Shin, W. Qiu, R. Jarecki, J. A. Cox, R. H. Olsson III, A. Starbuck, Z. Wang, and P. T. Rakich, "Tailorable stimulated Brillouin scattering in nanoscale silicon waveguides," Nat. Commun. **4**, 1944 (2013).
17. R. Van Laer, B. Kuyken, D. Van Thourhout, and R. Baets, "Interaction between light and highly confined hypersound in a silicon photonic nanowire," Nat. Photonics **9**, 199–203 (2015).
18. R. Van Laer, A. Bazin, B. Kuyken, R. Baets, and D. Van Thourhout, "Net on-chip Brillouin gain based on suspended silicon nanowires," New J. Phys. **17**, 115005 (2015).
19. E. A. Kittlaus, H. Shin, and P. T. Rakich, "Large Brillouin amplification in silicon," Nat. Photonics **10**, 463–467 (2016).
20. E. A. Kittlaus, N. T. Otterstrom, and P. T. Rakich, "On-chip inter-modal Brillouin scattering," Nat. Commun. **8**, 15819 (2017).
21. N. T. Otterstrom, R. O. Behunin, E. A. Kittlaus, Z. Wang, and P. T. Rakich, "A silicon Brillouin laser," Science **360**, 1113–1116 (2018).
22. T. Tanemura, Y. Takushima, and K. Kikuchi, "Narrowband optical filter, with a variable transmission spectrum, using stimulated Brillouin scattering in optical fiber," Opt. Lett. **27**, 1552–1554 (2002).
23. R. Pant, D. Marpaung, I. V. Kabakova, B. Morrison, C. G. Poulton, and B. J. Eggleton, "On-chip stimulated Brillouin scattering for microwave signal processing and generation," Laser Photon. Rev. **8**, 653–666 (2014).
24. Y. Souidi, F. Taleb, J. Zheng, M. W. Lee, F. Du Burck, and V. Roncin, "Low-noise and high-gain Brillouin optical amplifier for narrowband active optical filtering based on a pump-to-signal optoelectronic tracking," Appl. Opt. **55**, 248–253 (2016).
25. A. Choudhary, B. Morrison, I. Aryanfar, S. Shahnia, M. Pagani, Y. Liu, K. Vu, S. Madden, D. Marpaung, and B. J. Eggleton, "Advanced integrated microwave signal processing with giant on-chip Brillouin gain," J. Lightwave Technol. **35**, 846–854 (2017).
26. A. V. Kozlovskiĭ, "Detection of weak optical signals with a laser amplifier," J. Exp. Theor. Phys. **102**, 24–33 (2006).
27. C. Wolff, P. Gutsche, M. J. Steel, B. J. Eggleton, and C. G. Poulton, "Power limits and a figure of merit for stimulated Brillouin scattering in the presence of third and fifth order loss," Opt. Express **23**, 26628–26638 (2015).
28. B. Morrison, A. Casas-Bedoya, G. Ren, K. Vu, Y. Liu, A. Zarifi, T. G. Nguyen, D.-Y. Choi, D. Marpaung, S. J. Madden, and A. Mitchell, "Compact Brillouin devices through hybrid integration on silicon," Optica **4**, 847–854 (2017).
29. M. S. Kang, A. Butsch, and P. St.J. Russell, "Reconfigurable light-driven opto-acoustic isolators in photonic crystal fibre," Nat. Photonics **5**, 549–553 (2011).
30. C. G. Poulton, R. Pant, A. Byrnes, S. Fan, M. Steel, and B. J. Eggleton, "Design for broadband on-chip isolator using stimulated Brillouin scattering in dispersion-engineered chalcogenide waveguides," Opt. Express **20**, 21235–21246 (2012).
31. A. H. Safavi-Naeini, T. M. Alegre, J. Chan, M. Eichenfield, M. Winger, Q. Lin, J. T. Hill, D. E. Chang, and O. Painter, "Electromagnetically induced transparency and slow light with optomechanics," Nature **472**, 69–73 (2011).
32. N. T. Otterstrom, R. O. Behunin, E. A. Kittlaus, and P. T. Rakich, "Optomechanical cooling in a continuous system," Phys. Rev. X **8**, 041034 (2018).
33. A. Masood, M. Pantouvaki, G. Lepage, P. Verheyen, J. Van Campenhout, P. Absil, D. Van Thourhout, and W. Bogaerts, "Comparison of heater architectures for thermal control of silicon photonic circuits," in *10th International Conference on Group IV Photonics* (IEEE, 2013), pp. 83–84.
34. E. Giacoumidis, A. Choudhary, E. Magi, D. Marpaung, K. Vu, P. Ma, D.-Y. Choi, S. Madden, B. Corcoran, M. Pelusi, and B. J. Eggleton, "Chip-based Brillouin processing for carrier recovery in self-coherent optical communications," Optica **5**, 1191–1199 (2018).
35. K. Y. Song, M. G. Herráez, and L. Thévenaz, "Observation of pulse delaying and advancement in optical fibers using stimulated Brillouin scattering," Opt. Express **13**, 82–88 (2005).
36. Y. Okawachi, M. S. Bigelow, J. E. Sharping, Z. Zhu, A. Schweinsberg, D. J. Gauthier, R. W. Boyd, and A. L. Gaeta, "Tunable all-optical delays via Brillouin slow light in an optical fiber," Phys. Rev. Lett. **94**, 153902 (2005).
37. R. Pant, A. Byrnes, C. G. Poulton, E. Li, D.-Y. Choi, S. Madden, B. Luther-Davies, and B. J. Eggleton, "Photonic-chip-based tunable slow and fast light via stimulated Brillouin scattering," Opt. Lett. **37**, 969–971 (2012).
38. D. L. Sounas and A. Alù, "Non-reciprocal photonics based on time modulation," Nat. Photonics **11**, 774–783 (2017).
39. M.-A. Miri, F. Ruesink, E. Verhagen, and A. Alù, "Optical nonreciprocity based on optomechanical coupling," Phys. Rev. Appl. **7**, 064014 (2017).
40. J. Kim, M. C. Kuzyk, K. Han, H. Wang, and G. Bahl, "Non-reciprocal Brillouin scattering induced transparency," Nat. Phys. **11**, 275–280 (2015).
41. C.-H. Dong, Z. Shen, C.-L. Zou, Y.-L. Zhang, W. Fu, and G.-C. Guo, "Brillouin-scattering-induced transparency and non-reciprocal light storage," Nat. Commun. **6**, 6193 (2015).
42. Z. Shen, Y.-L. Zhang, Y. Chen, C.-L. Zou, Y.-F. Xiao, X.-B. Zou, F.-W. Sun, G.-C. Guo, and C.-H. Dong, "Experimental realization of optomechanically induced non-reciprocity," Nat. Photonics **10**, 657–661 (2016).
43. F. Ruesink, M.-A. Miri, A. Alu, and E. Verhagen, "Nonreciprocity and magnetic-free isolation based on optomechanical interactions," Nat. Commun. **7**, 13662 (2016).
44. S. Hua, J. Wen, X. Jiang, Q. Hua, L. Jiang, and M. Xiao, "Demonstration of a chip-based optical isolator with parametric amplification," Nat. Commun. **7**, 13657 (2016).

45. K. Fang, J. Luo, A. Metelmann, M. H. Matheny, F. Marquardt, A. A. Clerk, and O. Painter, "Generalized non-reciprocity in an optomechanical circuit via synthetic magnetism and reservoir engineering," Nat. Phys. **13**, 465–471 (2017).
46. Y. Shoji, T. Mizumoto, H. Yokoi, I.-W. Hsieh, and R. M. Osgood, Jr., "Magneto-optical isolator with silicon waveguides fabricated by direct bonding," Appl. Phys. Lett. **92**, 071117 (2008).
47. L. Bi, J. Hu, P. Jiang, D. H. Kim, G. F. Dionne, L. C. Kimerling, and C. Ross, "On-chip optical isolation in monolithically integrated non-reciprocal optical resonators," Nat. Photonics **5**, 758–762 (2011).
48. D. Huang, P. Pintus, C. Zhang, Y. Shoji, T. Mizumoto, and J. E. Bowers, "Electrically driven and thermally tunable integrated optical isolators for silicon photonics," IEEE J. Sel. Top. Quantum Electron. **22**, 4403408 (2016).
49. P. Pintus, D. Huang, P. A. Morton, Y. Shoji, T. Mizumoto, and J. E. Bowers, "Broadband TE optical isolators and circulators in silicon photonics through Ce:YIG bonding," J. Lightwave Technol. **37**, 1463–1473 (2019).
50. D. B. Sohn, S. Kim, and G. Bahl, "Time-reversal symmetry breaking with acoustic pumping of nanophotonic circuits," Nat. Photonics **12**, 91–97 (2018).
51. E. A. Kittlaus, N. T. Otterstrom, P. Kharel, S. Gertler, and P. T. Rakich, "Non-reciprocal interband Brillouin modulation," Nat. Photonics **12**, 613–619 (2018).